

PERFORMANCE MODELING OF A WIDE FIELD GROUND LAYER ADAPTIVE OPTICS SYSTEM

DAVID R. ANDERSEN¹, JEFF STOESZ¹, SIMON MORRIS², MICHAEL LLOYD-HART³, DAVID CRAMPTON¹, TIM BUTTERLEY², BRENT ELLERBROEK⁴, LAURENT JOLISSAINT¹, N. MARK MILTON³, RICHARD MYERS², KEI SZETO¹, ANDREI TOKOVININ⁵, JEAN-PIERRE VÉRAN¹, RICHARD WILSON²

¹NRC Herzberg Institute of Astrophysics, 5071 W Saanich Road, Victoria, BC V9E 2E7, Canada,

²Department of Physics, University of Durham, Rochester Building, Science Laboratories, South Road, Durham DH1 3LE, UK,

³Steward Observatory, University of Arizona, 933 North Cherry Avenue, Tucson, AZ 85721, USA,

⁴Thirty Meter Telescope Project, 1200 E. California Boulevard, Mail Code 102-8, Pasadena, California, 91125, USA,

⁵Cerro Tololo Inter-American Observatory, Casilla 603, La Serena, Chile

Draft version October 1, 2018

ABSTRACT

Using five independent analytic and Monte Carlo simulation codes, we have studied the performance of wide field ground layer adaptive optics (GLAO), which can use a single, relatively low order deformable mirror to correct the wavefront errors from the lowest altitude turbulence. GLAO concentrates more light from a point source in a smaller area on the science detector, but unlike traditional adaptive optics, images do not become diffraction-limited. Rather the GLAO point spread function (PSF) has the same functional form as a seeing-limited PSF, and can be characterized by familiar performance metrics such as Full-Width Half-Max (FWHM). The FWHM of a GLAO PSF is reduced by 0.1" or more for optical and near-infrared wavelengths over different atmospheric conditions. For the Cerro Pachón atmospheric model this correction is even greater when the image quality is worst, which effectively eliminates “bad-seeing” nights; the best seeing-limited image quality, available only 20% of the time, can be achieved 60 to 80% of the time with GLAO. This concentration of energy in the PSF will reduce required exposure times and improve the efficiency of an observatory up to 30 to 40%. These performance gains are relatively insensitive to a number of trades including the exact field of view of a wide field GLAO system, the conjugate altitude and actuator density of the deformable mirror, and the number and configuration of the guide stars.

Subject headings: instrumentation: adaptive optics

1. INTRODUCTION

The idea that the turbulence of the atmosphere can be corrected by adaptive optics (AO) is not new (Babcock 1953), but there have always been limitations to the approach. One of the more serious is that classical or single guide star AO systems produce only a small corrected field of view (FOV); isoplanatic errors cause the image quality to quickly degrade from the center of the corrected field; typically, the spatial resolution falls below the diffraction limit in the near-infrared only 30 arcseconds from the guide star. This small and non-uniform corrected FOV severely limits the sky coverage of traditional AO systems, and even limits sky coverage for those that employ Laser Guide Stars (LGSs; first proposed by Foy & Labeyrie 1985). Another limitation of traditional AO systems is that the performance decreases from the near-infrared to the visible; to fully correct the turbulence in the optical would require deformable mirrors (DMs) with many more actuators and a control system operating at a much higher frequency (Dekany 2006). Finally, existing AO systems perform well only when the image quality conditions are good; if the seeing is poor, control bandwidths and DM actuator strokes and densities are insufficient to maintain diffraction limited imaging.

In the near future, Multi-Conjugate Adaptive Optics (MCAO) systems (Johnston & Welsh 1991; Ragazzoni, 1999; Beckers, 2000; Ragazzoni, Farinato, & Marchetti 2000; Flicker, Rigaut & Ellerbroek 2000) promise to pro-

duce a larger corrected FOV with improved sky coverage, by employing multiple DMs and wavefront sensors (WFSs), but will still be limited to observations in the near-infrared on nights with average or better image quality. While the availability of MCAO systems will change the use of observatories, it is important to realize that today a large fraction of ground based astronomical research still relies on seeing limited observations at optical wavelengths. Ground layer adaptive optics (GLAO) was proposed to circumvent these limitations of traditional AO systems by applying a limited AO correction to an even larger FOV under any atmospheric conditions even at optical wavelengths (Rigaut 2002). A GLAO system does not attempt to produce diffraction limited images, but rather to improve the concentration of the point spread function (PSF) by sensing and correcting only the lowest turbulent layers of the atmospheres. Because the corrected layers are so close to the ground, the correction is the same over the entire large FOV. Uncorrected turbulent layers at higher altitudes degrade the spatial resolution isoplanatically. The use of GLAO can therefore complement MCAO surveys; the survey efficiency of a GLAO system, as we show, continues to increase as the FOV increases and actually surpasses that of a MCAO system. MCAO or classical AO can then be used for follow-up observations of individual discoveries made from GLAO surveys.

Early simulations suggested that GLAO could produce images with a Full-Width Half Maximum (FWHM) less than 0.2" in *J*-band. Caution should be used when evaluating early GLAO modeling results, however, be-

cause they are critically dependent on the input turbulence profiles. As Tokovinin (2004) points out, studies of GLAO require accurate knowledge of the atmosphere below ~ 2 km in addition to knowing the turbulence profile of the free atmosphere. Specifically, turbulent layers at intermediate altitudes which Tokovinin termed the “gray zone,” will only be partially corrected and will also introduce residual anisoplanatism. Earlier work on GLAO focused on FOVs less than 3 arcminutes (Baranec, Lloyd-Hart, Codona, Milton 2003; Tokovinin 2004; LeLouarn & Hubin 2004; Hubin *et al.* 2004; Jolissaint, Véran, & Stoesz 2004; Stoesz *et al.* 2004).

Here we examine the performance of a GLAO system over FOVs greater than 5 arcminutes in size using new, higher resolution turbulence profiles. This work was carried out to study the potential of a GLAO system at the *Gemini* Observatory, but the results are applicable to 10m-class telescopes in general. The results presented here are based on a set of model atmospheres that were derived at least in part from balloon measurements of the turbulence over Cerro Pachón which had a vertical resolution of 6m (Tokovinin & Travouillon 2006). After describing these model atmospheres in section 2, we present the analytic and Monte Carlo modeling tools used for this study in section 3. We also reconcile the results of these codes, which lends greater confidence in the results. Section 4 describes the GLAO PSF and relevant performance metrics. We apply these metrics in analyzing a baseline wide field GLAO system in section 5 and describe various trades on this baseline in section 6. Finally section 7 provides a summary of our modeling results and a discussion of the promising future of GLAO.

2. MODEL ATMOSPHERES

GLAO system performance depends crucially on the structure of the atmospheric turbulence profile. In particular, the size of the compensated field and the uniformity of the delivered PSF over the field depend on the thickness of the boundary layer, while the overall degree of image improvement depends sensitively on the ratio of aberrations in the boundary layer to those in the free atmosphere. Historically these are not quantities that have been studied in detail because, prior to the emergence of GLAO as a potentially valuable observing tool, they were not seen as important measures of a site’s quality.

Fortunately for our study, detailed measurements of the structure of the atmospheric turbulence with a resolution of 6m in the boundary layer (altitudes below 5000m) recorded from 43 balloon flights exist as part of the 1998 *Gemini-South* seeing campaign at Cerro Pachón (Vernin *et al.* 2000). The atmospheric turbulence profiles used in this study have been derived from those balloon data and MASS-DIMM data also from Cerro Pachón taken in 2003 (Tokovinin & Travouillon 2006; see also Tokovinin, Baumont, & Vasquez 2003). While more site testing is required to confirm the presence of strong ground layer turbulence at other sites, the results of GLAO simulations using the high resolution atmospheric data from Cerro Pachón should be generally applicable to other telescope sites.

In order to reduce the magnitude of the modeling task, a total of nine atmospheric profiles have been constructed from the balloon flight data that represent a broad range

TABLE 1
INTEGRATED TURBULENCE $J = \int C_n^2 dh$ IN $m^{1/3}$ FOR “GOOD,” “TYPICAL,” AND “BAD” GROUND AND FREE (ALTITUDES > 3KM ARE CONSIDERED “FREE”) ATMOSPHERES.

altitude (m)	Good $J (10^{-14} m^{1/3})$	Typical $J (10^{-14} m^{1/3})$	Bad $J (10^{-14} m^{1/3})$
0	9.26	7.04	13.8
25	1.83	2.25	10.8
50	0.574	1.35	15.3
100	0.362	1.24	15.8
200	0.614	1.99	10.3
400	0.960	2.87	6.46
800	1.18	3.02	7.29
1600	0.913	1.75	6.77
3600			32.0
5500		17.0	
8400	9.00		

of typical conditions. Three turbulence profiles for the atmosphere below 2km in altitude were computed, representing the averages of the 25% best, 25% worst, and central 50% of the data sorted by r_0 . Similarly the free atmosphere above 2 km was represented by a single layer of turbulence, with C_n^2 and height determined again from the best (25%), worst (25%), and typical (50%) conditions for the upper atmosphere. Essentially no degree of correlation between the strengths of the boundary layer and the free atmosphere were found (Tokovinin 2003), so nine profiles were constructed by matching the three boundary layer profiles with each of the three upper atmosphere layers. Table 1 gives the altitudes and integrated turbulence values ($J = \int C_n^2 dh$ in $m^{1/3}$) for each of these profiles. The first column of this table is the effective height of each layer above the site level, as defined by the integral $\int h C_n^2 dh / J$, and the remaining columns are the integrated turbulence values for each model profile. The lowest layer was assigned a height of zero in this study. The approximate probabilities of occurrence, given the percentiles that the profiles were drawn from, are given in Table 2. Figure 1 shows good agreement between the cumulative probability distribution from the model predictions to measurements made from *Gemini-South*. Hence the results of our simulations should be representative of the conditions at Cerro Pachón during the four, one-week balloon missions that took place in all four seasons of 1998. We refer to these nine atmospheric models as two word (or two letter) designations for the Ground and Free atmosphere profiles, respectively. Hence, Good-Typical refers to the model atmosphere consisting of the “Good” (i.e. largest r_0) ground layer profile and “Typical” (median r_0) free atmosphere profile. A caveat to the results presented here is that while the profiles exhibit a wide range of r_0 values, almost all have similar isoplanatic angles, θ_0 ; in all cases we assumed an outer scale of $L_0 = 30$ m (Table 3).

3. MODELING TOOLS

In assessing the expected performance of GLAO, five simulation codes written by four groups have been used. These were thoroughly tested and compared to each other to ensure a high degree of confidence in the results. Three codes implement analytic calculations, while the remaining two codes are full wave propagation Monte Carlo simulations. Analytic codes, which calculate an estimate of the long exposure AO-corrected PSF using the

TABLE 2
PROBABILITIES USED TO WEIGHT
ATMOSPHERIC MODELS

Free Atmosphere	Good	Typical	Bad
Good	0.0625	0.125	0.0625
Typical	0.125	0.250	0.125
Bad	0.0625	0.125	0.0625

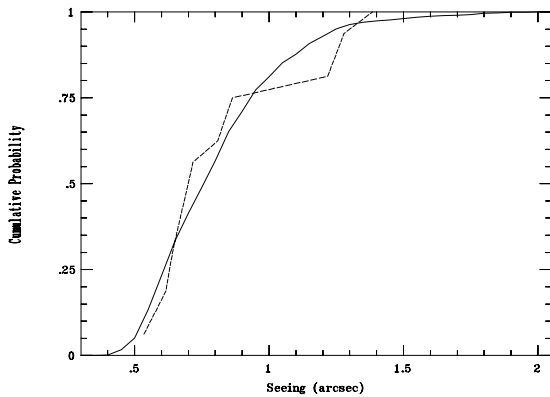


FIG. 1.— Cumulative histogram of *Gemini-South* seeing measurements in the *R*-band, with probabilities of the model atmospheric profiles over-plotted (dashed line). The measurements were made from *Gemini-South* acquisition camera data, corrected to zenith (Data available at <http://www.gemini.edu/metrics/seeing.html>). There is good agreement between these curves; the probabilities of the derived atmospheric profiles are within present experimental uncertainty.

fact that the optical transfer function is proportional to the negative exponential of the aperture averaged structure function of the residual phase disturbances in the telescope pupil, were generally used to explore large parameter spaces and study various performance trades. Monte Carlo models are much more computationally intensive, and were primarily used to study physical effects not incorporated into analytic models and to verify the analytic model results for the baseline configurations.

3.1. PAOLA Analytic Modeling Tool

One of the analytic modeling codes, PAOLA (Performance of Adaptive Optics for Large Apertures; Jolissaint, Véran 2002; Jolissaint, Véran, Conan 2006) was developed at NRC-HIA and is now used by more than a dozen groups throughout the world. It models the effect of the AO correction as a spatial frequency filtering of the turbulent phase power spectrum, from which the AO long exposure PSF in any direction is easily derived. One can identify five basic limitations on any classical AO system, and these are taken into account in the PAOLA code:

Anisoplanatism: in GLAO mode the DM commands are assumed to be derived from an average of the multiple guide star WFS measurements. The difference between this average command and the actual turbulent phase at a given point in the field is called the *anisoplanatic error*, and is described in (Stoesz *et al.* 2004) for the case of multiple natural guide star GLAO. It is important to note that this error term is by far the most important for GLAO;

Fitting error: The number of WFS lenslets (and/or DM actuators) defines the number of aberration modes that can be corrected by the system, and in particular sets the highest spatial frequency that can be measured and corrected. Uncorrected high spatial frequency aberrations are transmitted to the output of the AO system, giving rise to what is called the *fitting error*, due to the limited ability of the system to adjust (fit) itself to the incident phase. Fitting error is the next most important source of residual aberrations for GLAO;

WFS spatial aliasing: These same uncorrected high frequency aberrations are seen by the WFS as low spatial frequency errors, and are aliased in the low-frequency domain of the WFS. *Aliasing error* is the third important GLAO error source;

WFS noise: This error is due to the guide stars photon noise and WFS detector read noise and dark current noise;

System servo-lag: To achieve sufficient signal-to-noise on the phase measurement, the WFS has to integrate for a given exposure time. Determining the exposure time involves a trade-off between getting enough guide star photons and averaging out the high temporal phase fluctuations. Moreover, the reading of the WFS, the phase reconstruction and the DMs surface update takes some time (roughly one sampling period), creating a time-lag between phase measurement and correction. The phase error term associated to both time averaging and time-lag is called the *servo-lag error*;

The AO loop controller is modeled in PAOLA as a simple integrator. Such an analytical approach is very computationally efficient and permits PAOLA to model AO performance across large parameter spaces in a reasonable period of time. However, it can only account for the fundamental limits of the AO correction, so the performance estimates need to be refined with much more computationally intensive Monte-Carlo simulation tools (see sections 3.4 and 3.5), taking into account non-linear and/or second order effects (correlated effects, sensitivity to vibrations, cone effect, spot elongation, etc.), once a reduced set of suitable parameters has been found.

3.2. CIBOLA

CIBOLA (Covariance-Including Basic Option for Linear Analysis; Ellerbroek 2005) is a second analytical modeling tool that combines and extends features of PAOLA and prior analytical models for tomographic wavefront reconstruction and MCAO (Tokovinin 2001; Tokovinin 2002). This code may be used to assess the correlated effect of five fundamental error sources (DM fitting error; WFS spatial aliasing; WFS measurement noise; finite servo bandwidth; and anisoplanatism) for AO systems incorporating one or more deformable mirrors and wavefront sensors. Narrow and wide-field performance estimates may be obtained in terms of wavefront error power spectra and point spread functions, computed using either conventional, MCAO, or GLAO control algorithms.

TABLE 3
VALUES OF r_0 IN METERS, AND θ_0 AND SEEING IN ARCSECONDS AT 500NM FOR ALL NINE
 C_n^2 PROFILES USED IN THIS STUDY.

Free Atmosphere	Ground Layer						Bad		
	r_0 m	θ_0 "	Good	r_0 m	θ_0 "	Typical			
Good	0.189	2.61	0.535	0.164	2.59	0.616	0.083	2.52	1.218
Typical	0.157	2.72	0.644	0.141	2.70	0.717	0.079	2.62	1.279
Bad	0.125	2.84	0.809	0.117	2.82	0.864	0.073	2.73	1.385

The principal capabilities and limitations of CIBOLA are derived from the use of spatial filtering approximations for all of the basic wavefront propagation, sensing, reconstruction, and correction operators encountered in classical linear systems modeling of adaptive optics. This approach enables rapid analysis of AO systems which is sufficiently accurate for many applications, but is also neglects aperture edge effects and is (rigorously) limited to the case of natural guide stars.

3.3. Arizona analytic code

The idl-based analytic GLAO simulation tool used at the University of Arizona was originally developed by Tokovinin (2004). A multi-layer residual structure function for each beacon is computed from the von Karman power spectrum at each turbulent layer, accounting for the geometry of the beacon constellation. The model assumes that a single natural guide star is used for sensing global tilt. The effects of temporal delay and wavefront sensor noise are neglected.

3.4. Arizona Monte Carlo simulation code

The Monte Carlo simulation tool written at the University of Arizona, described by Lloyd-Hart & Milton (2003), supports an arbitrary number of LGS, natural guide stars (NGS), DMs, and atmospheric turbulence layers. The model assumes the geometric optics approximation. Atmospheric turbulence and DM corrections are represented as vectors of coefficients of the Zernike modes. An analytic computation is used to obtain the influence of atmospheric turbulence at each layer within the intersecting cone for each LGS and NGS. The net aberration for an object at infinity is also computed analytically.

The reconstruction matrix is built from the product of the maximum *a priori* (MAP) inverse of the DM influence matrix and the atmospheric layer influence matrix. Random turbulence Zernike coefficient vectors are generated from the Cerro Pachón atmospheric models using Kolmogorov statistics for Zernike order $1 \leq n \leq 30$ (*i.e.*, the first 496 Zernike polynomials). DM corrections are the product of these random turbulence Zernike coefficient vectors and the reconstruction matrix. Read noise with Gaussian statistics and Poisson photon noise are simulated for a Hartmann-Shack WFS and added to the noise-free wavefront corrections.

The performance of each candidate GLAO beacon configuration is evaluated by calculating the RMS wavefront deviation at a range of different field positions out to the full field radius. The expected uncorrected RMS error for Zernike modes of order $n > 30$ is added to account for high frequency modes not included in the simulation.

3.5. Durham Monte Carlo adaptive optics model

The University of Durham Monte Carlo AO model includes detailed WFS noise propagation and produces 2d PSFs, and was used to quantify the effects of such noise on PSF parameters across the GLAO field for various seeing and noise conditions and zenith angles. The capabilities of the UD Monte Carlo code are summarized as follows:

- The atmospheric model can cope with a large (not specifically-limited) number of independently moving turbulent layers.
- Multiple laser beacons and/or Natural Guide Stars can be modeled.
- Multiple DMs of a number of types can be modeled.
- Multiple Wavefront Sensors (one per laser beacon or NGS) can be included. These include all main detector noise effects, as well as the effects of detector pixellation and atmospherically-induced speckle.
- The science PSF may be sampled at a number of field points.

3.6. Direct Comparison of Results

Starting with the same inputs (Table 4), three figures of merit were computed for PSFs compensated with GLAO: FWHM, ensquared energy within $0.1''$, and Strehl ratio. Three turbulence profiles were run both with and without photon and read noise included. In all models, spatial fitting error was included, and some included WFS aliasing error. Other sources of residual wavefront error, such as servo lag, were omitted. The intention was not to produce realistic estimates of performance at *Gemini-S*, but merely to verify that the codes all predicted essentially the same results (this was not true initially, but excellent agreement was eventually achieved).

The results from the five codes are summarized in Figure 2 and demonstrate agreement to within $\sim 0.02''$ in the PSF FWHM. The two Monte Carlo codes generally predict somewhat worse performance than the three analytic codes, presumably because of the inclusion in the Monte Carlo simulations of a greater range of physical effects.

4. TOOLS FOR EVALUATING GLAO PERFORMANCE

The PSF from a GLAO system is very different from the PSF of a diffraction-limited AO system. Therefore, the proper merit functions for evaluating a GLAO system

TABLE 4
PARAMETERS OF THE COMMON MODELS USED TO VALIDATE THE SIMULATION CODES.

Atmosphere	$r_0 = 17$ cm at $\lambda = 500$ nm. $L_0 = 30$ m C_n^2 profiles (fractional power at each height): Height (m) 0 300 500 900 2000 10000 Profile 1: 0.45 0.15 0.00 0.00 0.07 0.33 Profile 2: 0.30 0.00 0.30 0.00 0.07 0.33 Profile 3: 0.20 0.00 0.00 0.40 0.07 0.33
Telescope	Outer Diameter = 8.0 m. No central obscuration
FOV	10' square
Guide Stars	5 NGS on a regular pentagon in a circle of radius 7'.07 Brightness: Case 1: infinite Case 2: $R=13$ (85,400 photon/m ² /s)
WFS	10×10 Shack-Hartmann, 8×8 pixels per subaperture Plate scale: 0.2" per pixel Read noise: 3.5 e ⁻ rms per readout per pixel Frame rate: 500 per second Wavelength: 700 nm monochromatic No sky background
DM	Conjugate height: 0 m Compensation: ≤ 77 degrees of freedom
Test stars	Co-ordinates: (0'.0, 0'.0) (2'.5, 0'.0) (5'.0, 0'.0) (2'.5, 2'.5) (5'.0, 5'.0) Wavelength: 1.25 μ m monochromatic Plate scale: 0''.1 per pixel Integration time: ≥ 100 s

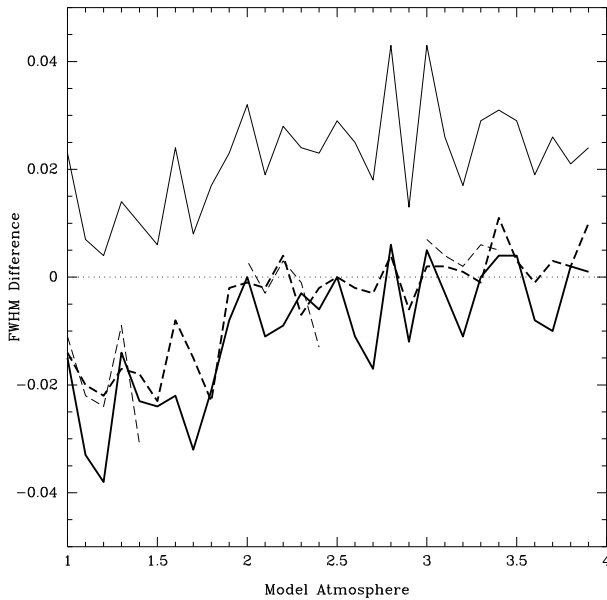


FIG. 2.— Difference in simulated FWHM between various simulations codes and the Durham Monte Carlo model for various model atmospheres, field positions, and treatments of noise presented in Table 4. The UA Monte Carlo code results are marked with a solid line (the residuals are all greater than 0), the UA Analytic code results are marked with a thin dashed line, the PAOLA results are marked with a heavy dashed line, and the CIBOLA results are marked with a heavy solid line. Results between 1-1.9 use Profile 1 from Table 4, results between 2-2.9 use Profile 2, and results between 3-3.9 use Profile 3. The ten PSF residuals shown for each profile are made from five field positions with and without the inclusion of noise. Results labeled with numbers greater than or equal to one half for each profile came from simulations including noise. For an absolute sense of scale, the Durham model FWHM for 1.0 is 0.235", 2.0 is 0.258", and 3.0 is 0.307". Regardless of the details of the fits, model atmospheres, or inclusion of noise, the five GLAO simulation codes produced FWHM which agreed to within 0.04". In most cases the agreement was even better. The analytic codes produced virtually indistinguishable results; the Monte Carlo codes, which included a greater range of physical effects, produced corrected FWHM which were not quite as narrow in most cases.

need to be identified. We begin this process by describing the functional form of the GLAO PSF and then present and discuss various performance metrics we use to gauge the performance of GLAO.

4.1. The GLAO Point Spread Function

The PSF produced by a wide-field GLAO system exhibits no diffraction-limited peak, and qualitatively is very similar to the PSF generated without any form of AO. The shape of the GLAO PSF shown in Figure 3 is well fit by the same function commonly used to describe seeing limited PSFs, the Moffat function (Moffat 1969):

$$I(r) = I_0[1 + (r/\alpha)^2]^{-\beta}. \quad (1)$$

A Gaussian profile matches the profile shape only to roughly the 50% of the peak flux, while the Moffat function provides a good fit below 1% of the peak height. Based on our simulated PSFs, both the GLAO PSF and seeing limited PSF are well fit by a Moffat PSF with β between 2.5 and 4.5.

4.2. GLAO Merit Functions

As part of the Gemini feasibility study, a reasonably detailed science case was prepared for GLAO. Science requirements for GLAO with representative instruments were then defined. Proper modeling of the science gains from a GLAO system require the full PSF information. However, for many of the science cases, a few key parameters were identified that gave a reasonable (but simplified) understanding of the gains. We present and discuss several of these merit functions here:

Full-Width-Half-Maximum (FWHM) of the PSF is a familiar and easily calculable quantity. For proper motion studies or work on crowded stellar fields, at least with the expected GLAO PSF shapes, FWHM is a key parameter.

Half light radius (θ_{50}), or the radius enclosing 50% of the total energy, is a particularly valuable merit

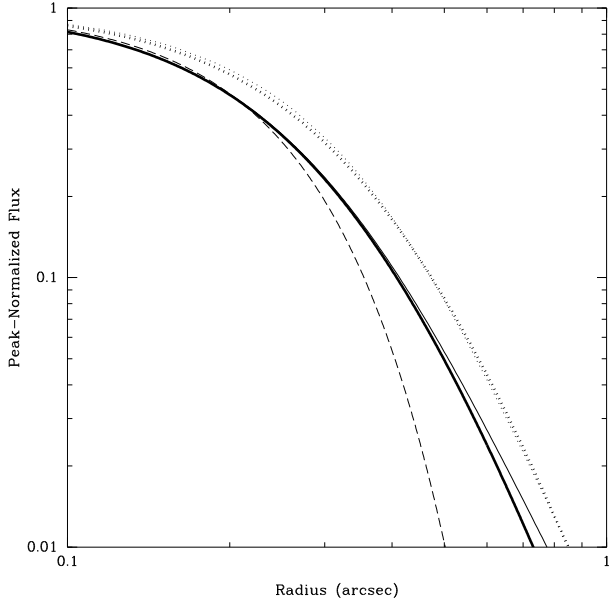


FIG. 3.— Radial profile of GLAO corrected PSF in normalized flux versus radius (Heavy solid line). The seeing-limited PSF is marked with a heavy dotted line (to the right of the heavy solid line). Gaussian (dashed line) and Moffat (thin solid line to GLAO PSF; thin dotted line to seeing-limited PSF) fits are marked as well. A Moffat function with $\beta = 2.9$ provides an excellent fit to both the GLAO and seeing-limited PSFs in this case. The PSF was generated at a wavelength of $1.0 \mu\text{m}$.

function if the shape of the PSF is not well understood. A correlation exists between θ_{50} and FWHM (Figure 4), but because of the variation in the Moffat parameter β , the half light radius may be a better general merit function, since it is more tightly correlated with the integration time ratio discussed below.

Ensquared Energy (EE) measured within an aperture (we used $0.1''$ and $0.2''$ apertures) is an important merit function for spectroscopy as it indicates the amount of energy that enters a slit of a given size. The EE within 100 or 200 mas is small at most scientific wavelengths, however, as shown by Figure 5.

Integration Time Ratio (ITR) is defined as the ratio of required exposure times to reach a given signal-to-noise ratio in the optimal aperture in the background limited case without and with GLAO; the higher the value of ITR, the greater the GLAO performance gain. ITR is especially relevant to science cases requiring faint, point-like object imaging. As expected from the Signal-to-Noise equation, ITR is proportional to the square of the ratio of seeing-limited to GLAO θ_{50} (Figure 6).

Image Quality Variation over the scientific FOV is an important scientific criterion to consider. In practical terms, PSF uniformity across the FOV will make observations easier to calibrate, reduce and interpret. As we will discuss later, however, image quality variation is critically dependent on the FOV being averaged (Figure 7). If areas near guide stars are included in the measure of image

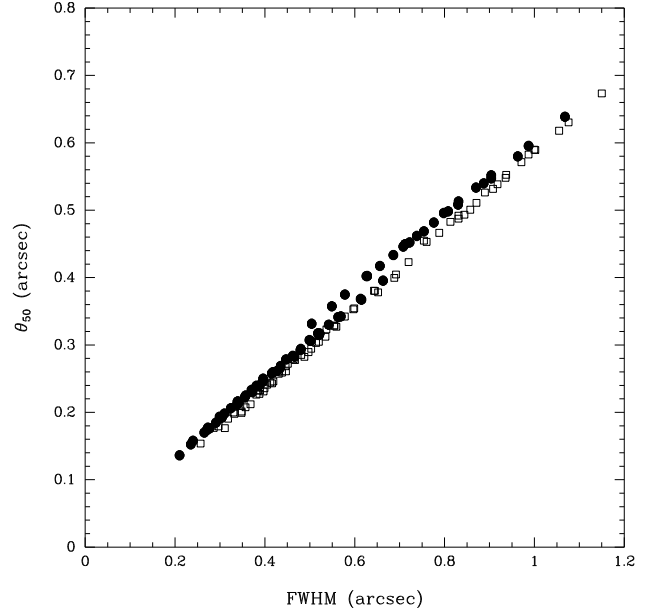


FIG. 4.— FWHM versus radius enclosing 50% of the total energy for a variety of wavelengths and turbulence profiles. The open squares are results for seeing-limited PSFs and the filled circles show results of GLAO-improved PSFs. The two parameters are strongly correlated which indicates that the shape (i.e., the Moffat β parameter) of the PSF does not change significantly in these simulations. There are two sequences apparent in the GLAO PSFs. The points in the upper sequence were simulated using the “Bad” ground layer turbulence profile. In this case, it appears that the core of the PSF is improved with GLAO, but that PSF halo is slightly stronger which leads to a comparatively larger half light radius. The overall tight relation between half light radius and FWHM means that both parameters are valuable GLAO merit functions.

quality variation, that variation will increase substantially. In general, image quality is very uniform over interesting FOVs.

Strehl Ratio, an important merit function for classical AO systems, is defined as the ratio of the PSF peak flux to the peak flux of the perfectly diffraction-limited PSF. However, Strehl Ratio has little meaning for a GLAO system; at the wavelength of $1.25 \mu\text{m}$, all codes predict less than 2% Strehl ratios (Figure 5).

For making general comparisons between the GLAO performance and seeing limited performance, the FWHM or θ_{50} are the most useful parameters. Ensquared energy is the most interesting merit function for a specific spectrograph slit size, but the gains measured from ensquared energies are very sensitive to the size of the slit aperture; very small absolute GLAO performance gains will be found if the aperture is significantly smaller than the FWHM, because very little light will make it through a narrow slit aperture in either the GLAO or seeing-limited case. The largest absolute and relative GLAO performance gain is found if the aperture size approaches the GLAO FWHM (Figure 5) which follows since the radial profile of the GLAO PSF is falling at the given aperture slit width while the radial profile of the seeing-limited PSF is still relatively flat and near the peak value. We therefore adopt the FWHM as the primary GLAO performance metric through the course of this work, and will cite EE or ITR only when relevant.

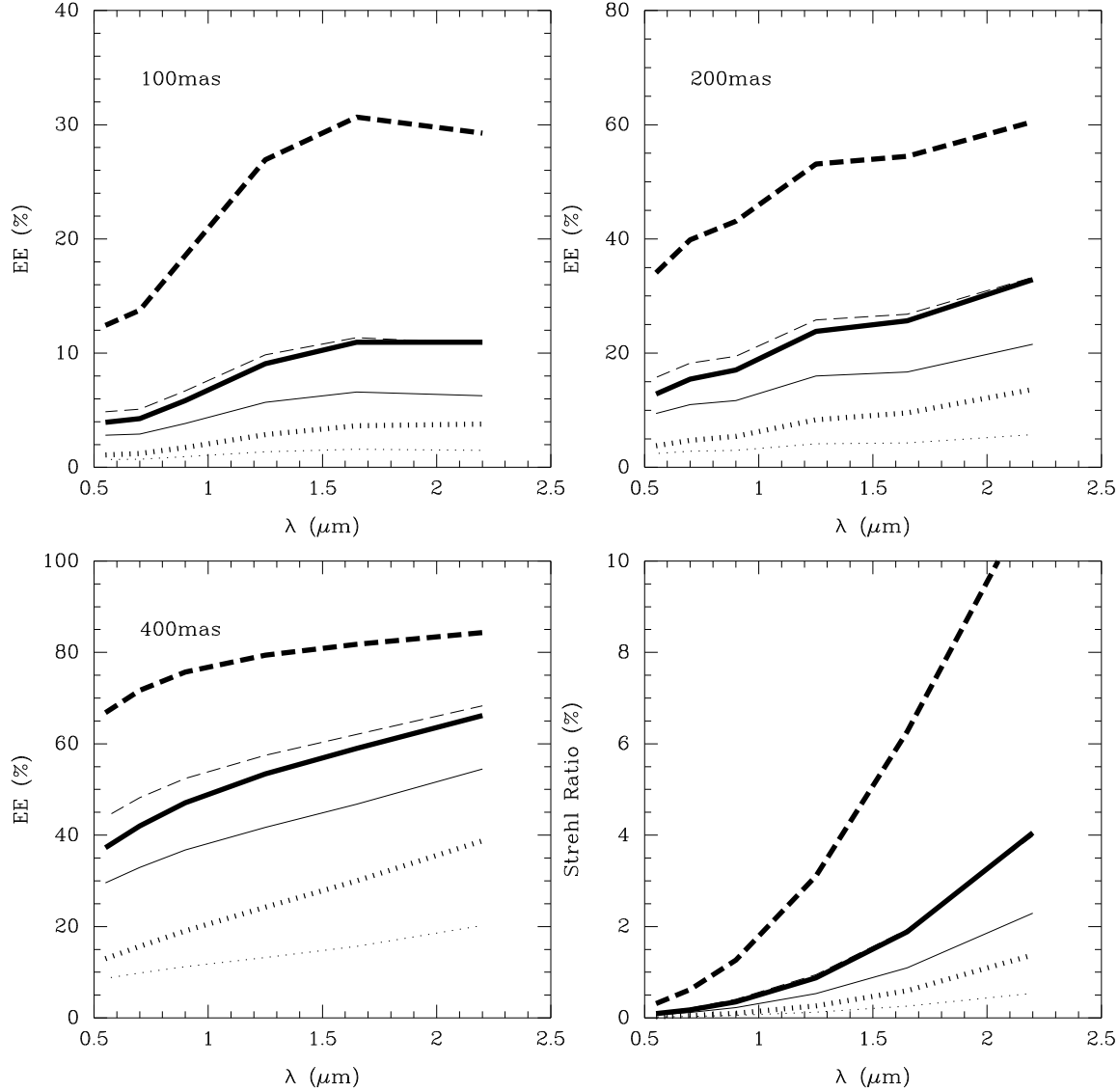


FIG. 5.— Ensquared energy within 100, 200 and 400 milli-arcseconds and Strehl ratio versus wavelength for B:B (dotted lines), T:T (solid lines), G:G (dashed lines). Heavy lines show the GLAO performance, while thin lines show the seeing limited measurements. The ensquared energy within 100mas is less than 10% at most wavelengths, and for most turbulence profiles. Only 20% of the ensquared energy is within 200mas in most cases. The Strehl Ratio is very low for wide field GLAO observations; the Strehl ratio is less than 4% in most cases (excepting the G:G performance at $\lambda > 1.5\mu\text{m}$).

5. PERFORMANCE OF A WIDE-FIELD GLAO SYSTEM

Based on initial results of the simulations, that showed that performance of GLAO systems are relatively insensitive to the specific LGS asterism and FOV (see section 6), a baseline GLAO configuration was adopted which employs four Sodium LGS arranged in a square, with each beacon 5 arcminutes from the center. When used, we adopt an asterism of three equally bright NGSs arranged in a triangle (Figure 8; NGSs used for correcting tip-tilt are only used in the Monte Carlo simulations). We used WFSs with a relatively small number of subapertures; only 10 to 17 samples across the diameter of the DMs or WFSs were used (between 77 to 227 total subapertures) depending on the simulation, because a high order correction is not necessary to achieve a good GLAO correction

(See section 6.2.1). We averaged the signal from the four LGS WFSs so the uncorrelated signal will cancel on average, leaving only the common signal from the ground layer. The deviations in wavefronts caused by layers over 2km will be uncorrelated. We modeled a GLAO system which employed an adaptive secondary mirror (first proposed by Beckers 1989) conjugated to -97m capable of correcting between 80 and 230 modes depending on the WFS architecture (-97m is the conjugate altitude of the current non-adaptive secondary mirrors of the *Gemini* telescopes. As section 6.2.2 shows, the results of simulations are relatively insensitive to the conjugate altitude.). The performance of the GLAO system was modeled at four scientific wavelengths: $0.7\mu\text{m}$, $1\mu\text{m}$, $1.65\mu\text{m}$, $2.2\mu\text{m}$ corresponding roughly to *RJHK*-bands.

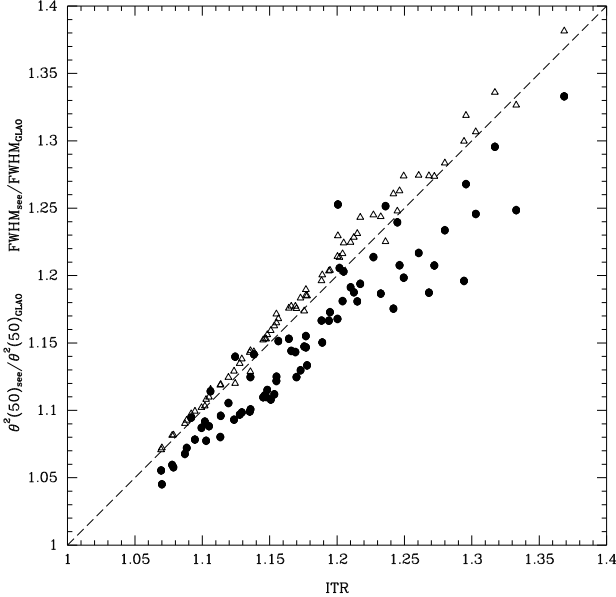


FIG. 6.— Integration Time Ratio (ITR) versus the ratio of seeing-limited to GLAO-corrected FWHM (closed circles) and the square of the ratio of seeing-limited to GLAO-corrected half-light radius θ_{50} (open triangles) for a range of wavelengths and turbulence profiles. While both FWHM and $(\theta_{50})^2$ ratios are good proxies for ITR, it should be noted that the correlation between ITR and $(\theta_{50})^2$ ratio is significantly tighter.

5.1. Image Quality Improvement

At all wavelengths studied and for most model atmospheres, we find that GLAO will decrease the FWHM of a PSF by roughly $0.1''$. However, the fractional change in PSF FWHM varies significantly from a factor of 3.8 improvement in the *K*-band with the Bad-Good profile, to just a factor of 1.1 improvement in the *R*-band with the Typical-Bad profile. The performance improvement is greatest when the ground layer turbulence is large (Figure 9). This means that the best image quality conditions which, without GLAO, occur only 20% of the time occur 60-80% of the time with a GLAO system, transforming the cumulative distribution of image quality (Figure 10). In particular, poor image quality conditions occur only rarely once a GLAO system is employed.

The expectation from previous studies (Rigaut 2002) was that the *J*-band GLAO FWHM should be roughly $0.2''$. As the results in Figures 9 and 10 show, the results presented here are more pessimistic. Simulations of the PSF using only the free atmosphere turbulence showed that even for a perfect GLAO correction the FWHM is greater than $0.2''$ under most atmospheric conditions. We note that the full GLAO simulation of atmospheres with “bad” free atmospheres yield smaller FWHM than from simulations of seeing-limited observations which included only the free atmosphere. This is due to the relatively low altitude of the “bad” free atmosphere (3km), which is being partially corrected by the GLAO simulations. Measured FWHM greater than $0.4''$ were initially attributed to a number of different factors, but as we show in section 6, the results are relatively insensitive to various trades. We believe the superior GLAO performance quoted previously can be primarily attributed to the adoption of simpler, more optimistic model at-

TABLE 5
PERFORMANCE OFF ZENITH FOR
TYPICAL-TYPICAL ATMOSPHERE FOR A
SCIENTIFIC WAVELENGTH OF $1.6\mu\text{m}$.

Zenith Angle	FWHM mean ('')	FWHM rms ('')	0.2'' EE mean	0.2'' EE rms
0°	0.299	0.013	0.211	0.006
30°	0.338	0.012	0.177	0.006
45°	0.401	0.012	0.137	0.004
60°	0.548	0.015	0.083	0.003

mospheres. The larger number of ground layers for our model atmospheres combined with the probabilities of given atmospheric conditions occurring, produce more realistic estimates of GLAO performance gains (which are still significantly improved over the seeing-limited performance).

Despite these lower estimates of GLAO-corrected FWHMs provided by our models, the gains in observing efficiency are still dramatic. Assuming background limited imaging and an optimal point source extraction radius, one can combine the GLAO gains using the model atmosphere probabilities listed in Table 2 to estimate GLAO efficiency gains between 1.5 and 2.0 at different scientific wavelengths (Figure 11). This can translate into a substantial gain for an observatory; based on the Gemini Observatory 2004B proposal statistics, GLAO would benefit 55% of the programs (proposals requesting observations between 0.6 and $2.2\mu\text{m}$ that do not require high order AO) and would improve the efficiency of the whole observatory by a factor up to 30% to 40%.

5.2. Performance Off Zenith

The performance off-zenith was studied assuming bright natural guide stars with the Typical-Typical atmospheric profiles. Field quadrant averages and standard deviations are given for all parameters measured at a wavelength of $1.6\mu\text{m}$ in Table 5. As expected, the performance decreases off zenith. The GLAO-corrected FWHM varies as a power-law of airmass with an exponent of 0.875, while the power-law without AO is 0.6. GLAO performance will always degrade with increasing airmass faster than the seeing-limited case because GLAO includes fitting error. Fitting error increases at the same rate as seeing plus anisoplanatism and will therefore degrade rapidly as more layers move into the grey zone described by Tokovinin.

5.3. Laser Power Requirements

The Durham Monte Carlo modeling tool was used to estimate the laser power requirements for a GLAO system. Figure 12 shows that a minimum flux of approximately 50 detected photons per WFS sub-aperture per detector integration will be required to achieve close to optimal correction. We note that the model considered the LGSs to be point sources and did not include spot elongation. Treating laser beacons as point sources results in simulated WFS spots which are too small and are thus accurately centroidable with fewer photons, so the predicted AO performance at low light levels is overly optimistic. With this caveat, we found that for 227 total subapertures, a sodium laser beacon and typical sodium

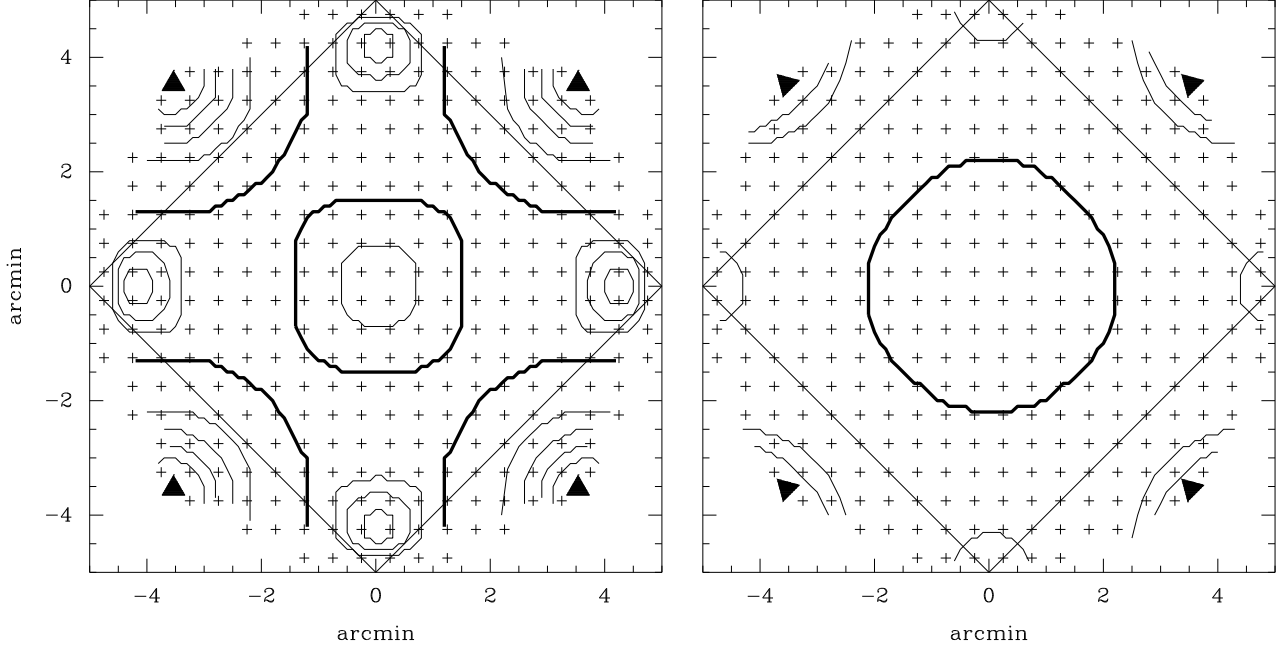


FIG. 7.— Ensquared Energy in $0.2''$ (EE; Left Panel) and FWHM (Right Panel) contours of GLAO PSF for the Good-Good turbulence profile as measured at $2.2\mu\text{m}$. A 7×7 square arcminute FOV is marked, as are each of the points simulated using PAOLA (+). LGS locations are marked with filled triangles. The performance is very uniform across the FOV; the separations between contours is just 1% in EE and $0.01''$ in FWHM. The thick lines correspond to contours of lowest EE in $0.2''$ (49%) and largest FWHM ($0.19''$). Near a LGS, the wavefront error will be reduced because the average of the pupils will be more heavily weighted by the turbulence from the free atmosphere in the direction of the LGS, thus leading to an improvement in image quality. Then, as one moves away from the direction of a LGS beacon, the performance will drop due to anisoplanatism. However, in the direction between two LGS, the total wavefront error will again decrease (and image quality improve) because now the wavefront error due to free atmosphere turbulence in that direction will be measured by two LGS WFS, and will not cancel. In the center of the FOV, the image quality will again improve very slightly as all 4 LGS WFS will sense a fraction of the turbulence from higher layers. In essence, the “grey zone” is field-dependent and is slightly higher in the field center, so more turbulence is corrected. If the scientific FOV can be chosen such that the LGSs are out of it, the correction across the FOV will be very uniform which makes data reduction and calibration easier.

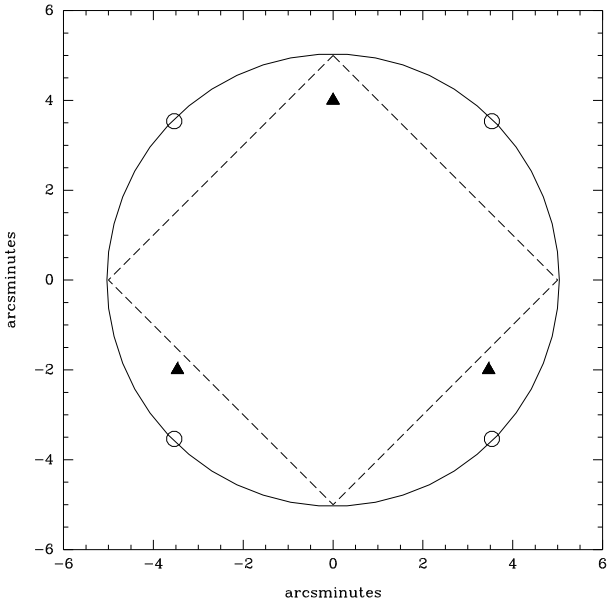


FIG. 8.— The geometry of the baseline GLAO system consists of 4 LGS marked with open circles on 5arcmin ring (solid line). 3 NGS are marked with closed triangles, and a 7×7 arcminute science FOV is marked with a dashed line.

layer column density, this translates to a LGS launch power less than 1 Watt. Even though this is a lower limit on the required laser power, sufficient WFS pho-

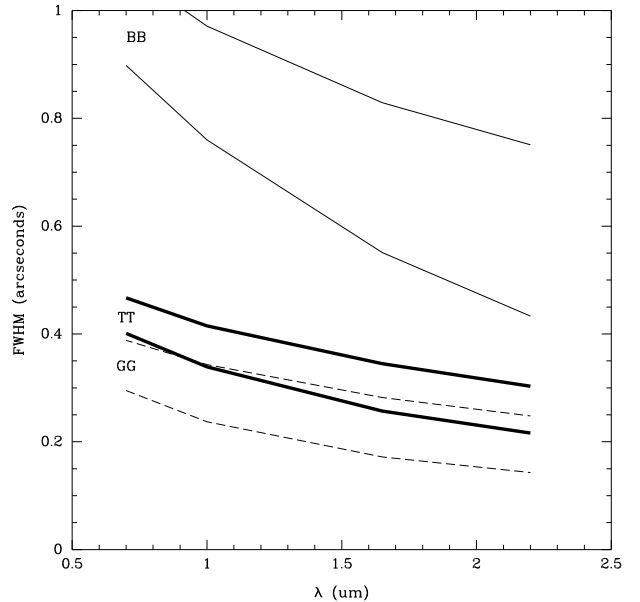


FIG. 9.— FWHM versus wavelength, λ , for three model atmospheres: Good-Good (dashed lines), Typical-Typical (heavy solid line) and Bad-Bad (thin solid line). The upper line is the seeing-limited FWHM and the lower line is the GLAO-corrected FWHM. The correction is greatest for turbulence profiles with Bad ground layers and at longer wavelengths. Simulations used a DM with 77 degrees of freedom and a 10 arcminute FOV.

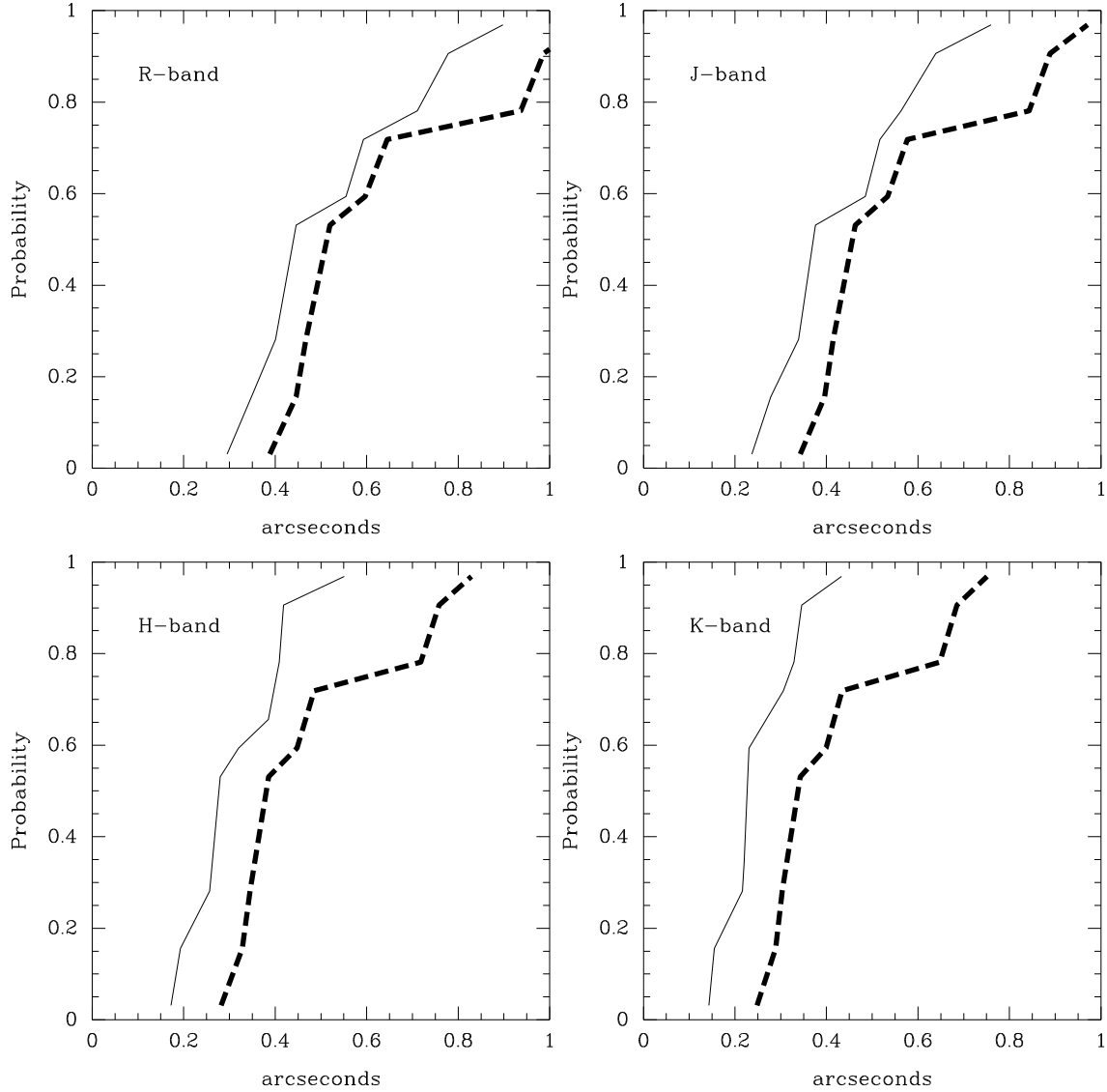


FIG. 10.— Cumulative histogram of FWHM based on the nine model atmospheres for both seeing-limited (heavy dashed lines) and GLAO (thin solid lines) cases for wavelengths of $0.70\mu\text{m}$ (*R*-band; upper left panel), $1.00\mu\text{m}$ (*J*-band; upper right panel), $1.65\mu\text{m}$ (*H*-band; lower left panel) and $2.2\mu\text{m}$ (*K*-band; lower right panel). All simulations used a DM with 77 degrees of freedom and a 10 arcminute FOV. A GLAO correction can alter the image quality statistics at a site; the relatively greater improvement when seeing is worst (and presumably the ground layer turbulence is greatest) means GLAO can virtually eliminate bad-seeing nights; the poorest image quality occurring 30% of the time without GLAO will only occur $\sim 10\%$ of the time with GLAO.

ton flux should be achieved with a relatively low power 2 to 5 Watt Sodium LGS system. The main reasons why the required power is low compared to other Laser AO systems is that the WFS signal is averaged, and the error budget for reaching the expected GLAO correction is relaxed; a GLAO system does not produce diffraction-limited images even in the near-IR so the required laser power is minimal.

5.4. Sky Coverage

To compute the sky coverage expected for our baseline system we used conservative estimates of the NGS noise performance drawn from our Monte Carlo simulations (Figure 13), and assumed: 1) 100 photons per integration are required, 2) GLAO used a 500Hz sampling rate, 3) the overall telescope plus detector efficiency was 60% and 4) the WFS operated in the V-band. Based on these

assumptions, one needs 3 NGS stars with $V < 15.0$ ¹. Based on the Bahcall and Soneira (1980) models of the Galaxy, there is a density of ~ 135 stars per square degree at the Galactic pole. For each third of the 70 square arcminute FOV, there will be an average of 0.9 stars per sector patrolled by the NGS WFS. Assuming the number of stars are Poisson distributed and spaced randomly over the FOV, there is a 20% probability that all 3 NGS WFS probes can be placed on $V < 15$ guide stars and a 81% chance that at least one probe can be placed on a bright NGS and the other two probes placed on fainter NGS

¹ The sampling rate of 500Hz was chosen only so that GLAO could be used to remove potential telescope vibrations. If these vibrations are unimportant, a sampling rate of 100Hz can be adopted which leads to a limiting magnitude for the NGS tip-tilt stars of $V < 16.8$.

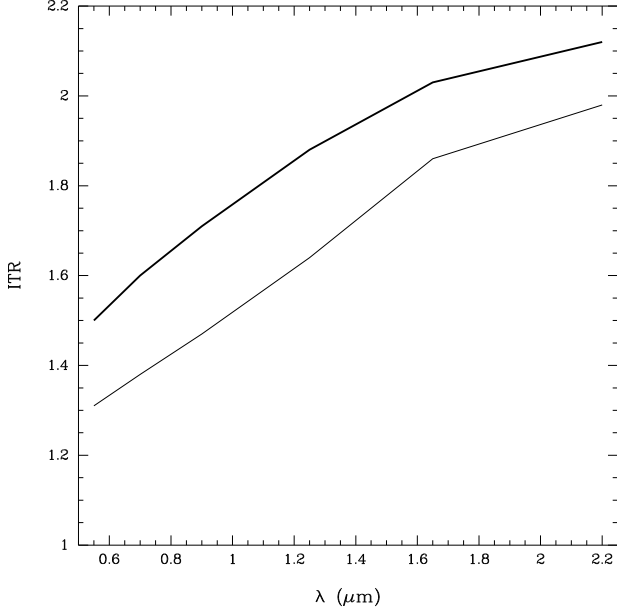


FIG. 11.— Integration Time Ratio (ITR) as a function of wavelength using DMs with 227 degrees of freedom (light line) and 2000 degrees of freedom (heavy line). This second, hypothetical DM with an enormous number of actuators represents the limit of ITR gain with a GLAO system. ITR was calculated by using a weighted sum over the nine turbulent profiles (See Table 2). Increasing the actuator density can significantly increase the performance of a GLAO system.

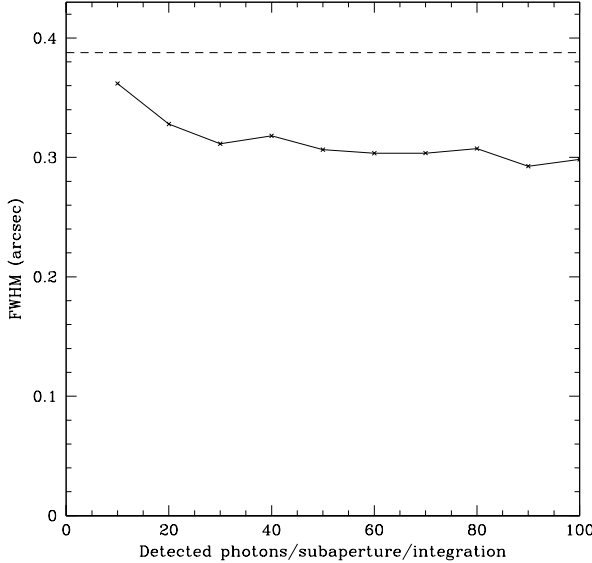


FIG. 12.— FWHM of science PSF at 1.6 microns as a function of LGS photon flux. Tip/tilt NGSs are assumed to be bright. The broken line shows the FWHM of the uncorrected PSF. The Monte Carlo simulations assumed the LGSs were point sources. Smaller spots are easier to centroid, therefore requiring fewer photos per subaperture to be centroidable. Larger, elongated spots will require more detected photons per subaperture, making this result a lower limit on the required photos to be produced by the LGSs.

read out at a slower rate (100 Hz). Only one NGS needs to be bright enough for the WFS to be read out rapidly and control telescope vibrations and wind shake; the gain from having 3 NGS versus 1 NGS WFSs reading out at such a fast rate will be significantly less substantial.

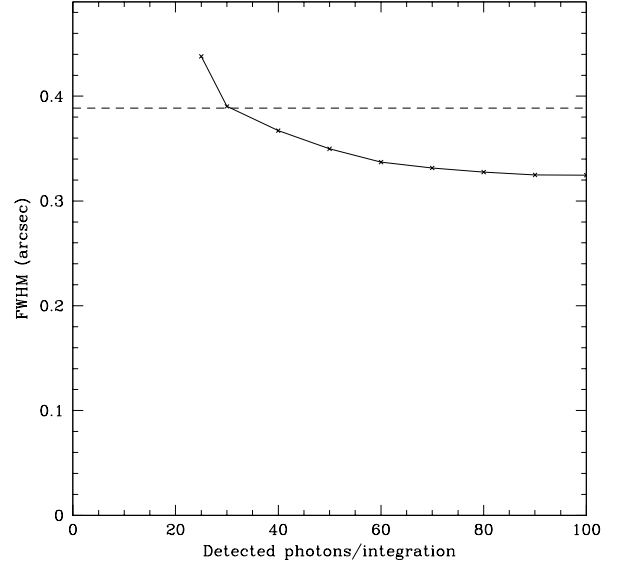


FIG. 13.— FWHM of science PSF at 1.6 microns as a function of NGS (tip/tilt) photon flux. LGSs are assumed to be bright. The broken line shows the FWHM of the uncorrected PSF. A GLAO system requiring 100 photons/integration with one WFS operating at 500 Hz translates into a 81% sky coverage at the North Galactic Pole (92% sky coverage is achievable with slightly diminished performance if only 60 detected photos per integration are required).

As shown in Figure 7, the non-uniformity of PSFs across the FOV is greatest near the LGSs. NGSs have a lesser effect on the variation of PSFs (Figure 14); the variation in PSFs introduced by NGSs is only apparent under the best atmospheric conditions. In general the PSF uniformity is still quite high over the selected FOV.

6. TRADE STUDY SIMULATIONS

Starting from this baseline model, we explore a large parameter space and track GLAO performance. We study how the performance of a GLAO system depends on the corrected field of view, the DM actuator density (or equivalently in our view, the WFS sampling), and different choices relating to the wavefront sensors. Because we wanted to study these trades over a range of relevant scientific wavelengths and the nine model atmospheres, we primarily used analytic modeling tools to carry out this work.

6.1. Field of View Trade Study

Our analytic simulations show that the GLAO performance does improve as the FOV (i.e., the radius of the LGS asterism) decreases, but the dependency between FOV and performance is weak; the FWHM decreases by only 18% when the area of the FOV is increased by a factor of 6.25 (Figure 15). This is not too surprising as MCAO systems, which also compensate for turbulence in discrete layers, exhibit only weak dependencies on the size of the FOV (e.g. Le Louarn 2002). The factor limiting GLAO performance gains is the strength of turbulence in the free atmosphere; a simulation of the atmosphere excluding the ground layer (all layers under 1.6 km), showed that the mean seeing of a perfect GLAO system will only be 0.28 arcseconds for a wavelength of $1\mu\text{m}$ assuming the simulated atmospheres and their weighted probabilities (Table 2) are reasonable, compared to the mean seeing without any adaptive optics of $0.56''$.

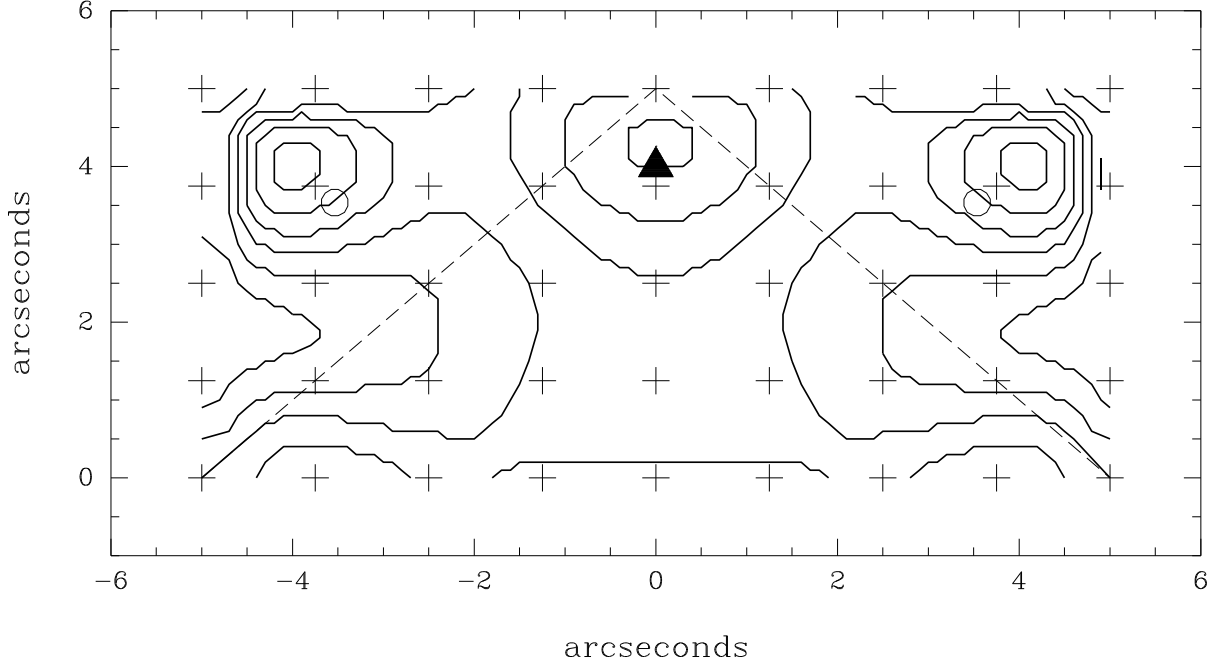


FIG. 14.— Contour plot showing FWHM for Monte Carlo simulation incorporating both LGS and low order NGS WFSs as measured at $1.65\mu\text{m}$ for the Good:Good turbulence profile (which shows the strongest variations in FWHM at this wavelength). LGSs are marked by open circles, and the location of the NGS is marked with a filled triangle. Locations of simulated points are marked with plus signs. Contours are separated by $0.05''$ steps in FWHM. The GLAO correction is slightly improved (by $0.1''$) at the location of the NGS when compared to the field center.

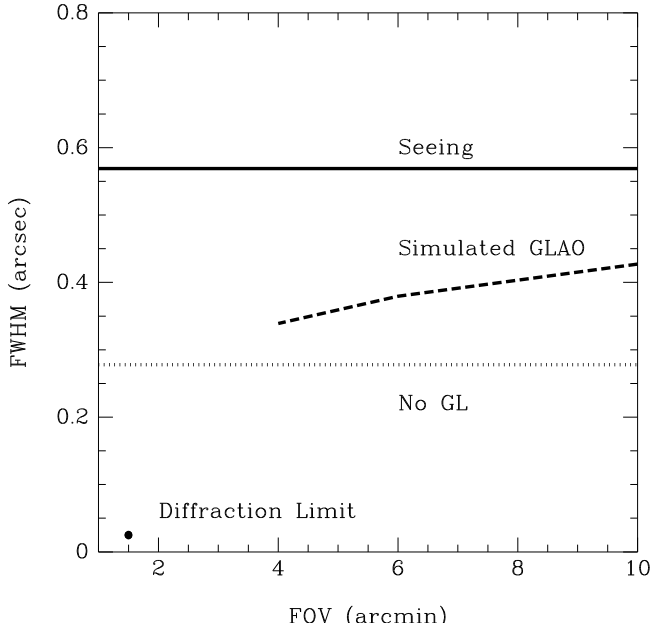


FIG. 15.— FWHM as measured at $1\mu\text{m}$ as a function of the FOV using the Typical:Typical turbulence profile. While the GLAO performance improves as field size shrinks, the gains are small; reducing the area of the FOV by a factor of 6.25 only improves the FWHM by 18%.

Even though the performance of a GLAO system decreases as the size of the corrected FOV increases, the overall survey efficiency (exposure time needed to survey a given area of the sky to a given limiting magnitude) increases. Since many of the primary science cases for MCAO and GLAO systems involve large surveys, we compared the relative survey efficiencies for these AO systems. The proposed Gemini GLAO imaging FOV is

49 square arcminutes compared to 2 square arcminutes for GSAOI, the imager for the Gemini MCAO system. For this example, the survey efficiency of a GLAO system is 4 times that of a MCAO system for point sources. For non-point sources, the ratio of observing efficiency increases dramatically; for objects with FWHM of 0.3 arcseconds, GLAO has an observing efficiency 40 times that of MCAO². Because this measure of survey efficiency does not include acquisition and setup times, real gains in observing efficiency are even greater when the additional overhead of setting up 25 MCAO observations to cover the same FOV as a single GLAO observation is taken into account. For planned GLAO systems, this result suggests that the GLAO FOV be made as large as possible, until the extra acquisition overhead associated with running a LGS GLAO system coupled to decreasing performance gain outweighs the increased FOV.

6.2. DM Property Trade Studies

6.2.1. Actuator Density

Another important dimension of the GLAO parameter space which we studied was the effect of varying actuator densities on GLAO performance. Initial simulations used a DM with 77 degrees of freedom. If the actuator density of the DM were significantly increased, we postulated that the performance may improve substantially because the fitting error would decrease. We found that the optimal number of actuators depends on both the turbulence profile and the scientific wavelength. In most cases the optimal number of actuators is actually quite large (~ 30 actuators across the DM or ~ 700 degrees of

² To be fair, MCAO will yield better angular resolution for these objects enabling more science than a mere detection.

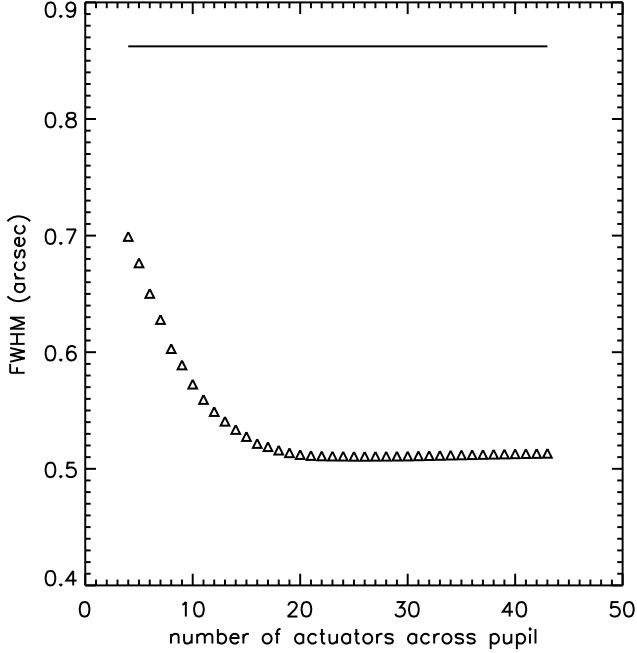


FIG. 16.— As a function of the number of degrees of freedom across the diameter of a DM, the FWHM at the field center is plotted as triangles. The solid horizontal line marks the seeing limited FWHM. Simulations were performed using the Bad:Good profile and 4 LGS at a radius of 5 arcminutes at a wavelength of 1 micron.

freedom). However, the performance in general is relatively insensitive to the number of actuators (Figure 16). Only 314 degrees of freedom are needed to recover 95% of the optimal GLAO performance for $\lambda > 0.7\mu\text{m}$. As figures 11 and 17 show, increasing the number of actuators has the greatest relative impact at the shortest scientific wavelength and when the free atmosphere has very little turbulence. In both these cases, fitting error dominates over other sources of error. If the goal of a GLAO system were only to deliver improved performance in the NIR, a DM with ~ 80 degrees of freedom would be adequate under most conditions.

6.2.2. Conjugate altitude of DM

If the DM in a GLAO system is conjugated to an altitude different than the effective height of the ground layer turbulence, one would expect anisoplanatism to degrade performance. However, analytic simulations of a DM that is not precisely conjugated to the ground layer atmospheric altitude show that the performance does not suffer significantly; at worst a 5% increase in FWHM is observed for the Gemini telescopes (Figure 18). We find that for a configuration of guide stars arranged in a pentagon, the optimal conjugation height is $\sim 100\text{m}$ considering all results at 1 to $2.2\mu\text{m}$ and all nine model profiles. Comparing the NGS pentagon to the LGS pentagon, we see that the constraint on GLAO performance from DM conjugate height misregistration is relaxed because of the cone effect. This is an important result, because it means that adaptive secondary mirrors can be used with Cassegrain telescopes³, such as the *Gemini*

³ The secondary mirror of a Cassegrain telescope is conjugated to below the primary mirror. For Gemini, the secondary is conjugated to 97m below the primary.

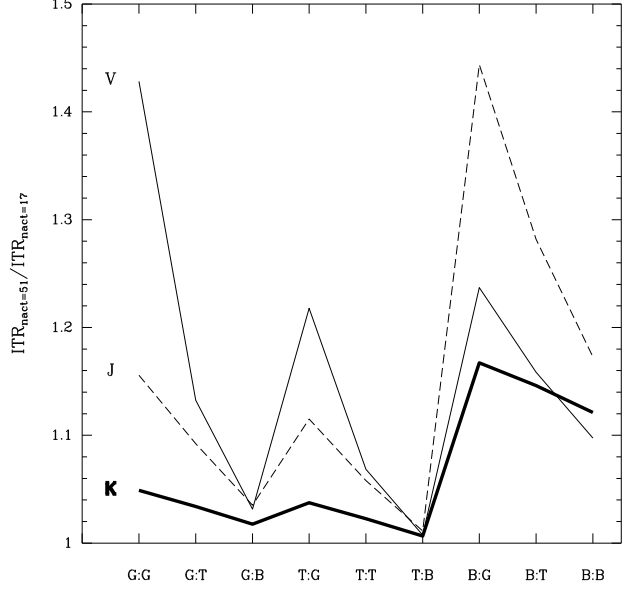


FIG. 17.— Ratio of Integration Time Ratio (ITR) calculated using DMs with 2000 (nact=51 across diameter) versus 227 (nact=17 across diameter) degrees of freedom as a function of the different turbulent profiles (labeled Ground Layer:Free Atmosphere) for VJK-bands ($0.55, 1.25, 2.2\mu\text{m}$). The gain at K-band is slight because 227 actuators are sufficient to correct the ground layer turbulence for all profiles. This is not the case in J-band, where it is clear 227 actuators are not sufficient to correct all the “Bad” ground layer turbulence. Increased actuator density improves GLAO performance for “Good” ground turbulence the most at shorter wavelengths. Even 2000 actuators across the DM are probably insufficient to correct the “Bad” ground layer turbulence in V-band, thereby limiting the gain in this regime.

telescopes, and still produce GLAO performance gains.

6.3. Guide Star Trade Studies

6.3.1. Laser versus Natural Guide Stars

We find that the GLAO performance is not optimal if all wavefront sensing is done using NGSs. For four real asterisms of NGSs near the North Galactic Pole, the mean and standard deviation of the PSF FWHM were calculated. Variations in the PSF are 5% greater over the FOV if NGS versus LGS asterisms are used.

For one GLAO simulation using 3 NGSs, we looked at the morphology of the PSF in greater detail. A comparison of the FWHM for the NGS and LGS system show again that the uniformity of the PSF FWHM is much higher for the LGS system (Figure 19); the standard deviation in FWHM is 34 mas in this NGS GLAO simulation compared to 8 mas for the LGS GLAO simulation. Furthermore, the correction yields an improvement in FWHM of only $0.05''$, roughly half the correction achieved using the LGS system. We measured ellipticity (one minus the axis ratio) of the isophotes corresponding to the radius of the FWHM. The magnitude and variation in ellipticity for the LGS simulation was small; the mean ellipticity is only 0.02. The change in shape of the PSF is roughly 2%. With NGSs alone, ellipticity becomes more significant; a mean ellipticity of 0.10 is observed (Figure 19). Ellipticity is a second order deviation — “higher order” deviations to the PSF shape appear to be negligible. Perhaps some of these disadvantages associated with using NGSs could be alleviated if even more

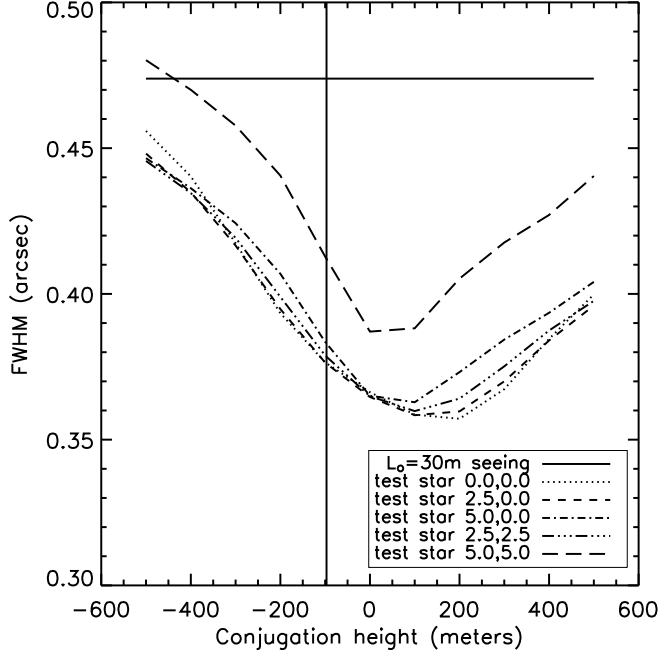


FIG. 18.— As a function of DM conjugation height, the FWHM of 5 field positions plus the seeing limited case (see legend). FWHM were measured from the Typical:Typical profile at a wavelength of 1 micron. Considering the five field positions, the optimal conjugate altitude, depending on the image quality criteria, is around +100m. The conjugation of the Gemini telescope secondary mirror is indicated by the vertical line at -97m, which suffers only a 5% degradation in FWHM relative to the optimal FWHM for this case.

NGSs are averaged and an optimal reconstruction algorithm were used (Nicolle *et al.* 2006).

Of course one other major advantages of using LGS versus NGS WFSs is that, as discussed in section 5.4, almost complete sky coverage can be achieved for a GLAO system using NGS to correct only the tip-tilt.

6.3.2. Number and Geometry of Laser Guide Stars

We explored GLAO performance for a range of guide star numbers and geometries. Cone effect and the altitude of the beacons were not included, which simplified the model and set aside the question of the relative placement of the high-order beacons and tip-tilt beacons that must be addressed with LGSs. Guided by the theoretical result of Tokovinin (2004) that the ideal beacon geometry for GLAO is a complete ring at the edge of the FOV, regular polygons, with and without an additional axial beacon, were explored from a triangle to a heptagon. For comparison, a single axial beacon was also investigated.

As Table 6 shows, more beacons yield slightly better results, as expected. Most of the performance gains are obtained by going from 1 to 3 LGSs. The addition of extra beacons only marginally improves the result when four or more beacons are employed. This is consistent with results reported from MCAO modeling (Fusco, *et al.* 1999). Adding more beacons in a GLAO system means that turbulence from high layers cancels out better because more non-overlapping high layer turbulence volumes are measured by the WFSs. We suspect the cancellation of high layer turbulence in the mean wavefront improves as the square root of the number of beacons.

TABLE 6
FIELD-AVERAGED FWHM IN ARCSEC FOR EACH GUIDE STAR GEOMETRY USING THE GOOD:GOOD, TYPICAL:Typical AND BAD:BAD CERRO PACHÓN TURBULENCE PROFILES.
MEASUREMENTS WERE MADE FOR A SCIENTIFIC WAVELENGTH OF $1\mu\text{m}$ AND A 10 ARCMINUTE DIAMETER FOV. GUIDE STARS ARE EVENLY SPACED AROUND THIS DIAMETER, UNLESS THE CONFIGURATION IS DENOTED, E.G. 3+1, IN WHICH CASE ONE LGS IS LOCATED AT THE CENTER OF THE FOV.

Guide Star Geometry	Good:Good	Typical:Typical	Bad:Bad
1	0.293 ± 0.027	0.471 ± 0.043	0.845 ± 0.070
3	0.230 ± 0.007	0.382 ± 0.012	0.727 ± 0.017
3+1	0.217 ± 0.008	0.361 ± 0.014	0.696 ± 0.025
4	0.221 ± 0.006	0.368 ± 0.009	0.708 ± 0.014
4+1	0.212 ± 0.007	0.354 ± 0.011	0.687 ± 0.021
5	0.215 ± 0.006	0.359 ± 0.009	0.694 ± 0.013
5+1	0.209 ± 0.006	0.348 ± 0.010	0.678 ± 0.018
6	0.212 ± 0.003	0.354 ± 0.004	0.688 ± 0.007
6+1	0.207 ± 0.004	0.346 ± 0.007	0.674 ± 0.015
No GLAO	0.351	0.474	0.992

6.3.3. Rayleigh versus Sodium Beacons

A comparison of the GLAO performance was made where the only difference was a change in beacon height appropriate for Rayleigh and Sodium lasers. There is at best a 5% improvement if Rayleigh beacons are used, corresponding to a relatively constant ~ 8 mas decrease in FWHM for the model turbulence profiles. This advantage stems from the fact that the cone effect from the lower Rayleigh beacon will be greater and thus be less affected by high turbulence layers.

6.3.4. Number of Tip-Tilt Stars versus Angular Resolution

For a LGS WFS system, tip-tilt sensing is typically done with NGS. Given the effects of anisoplanatism, a single star is inadequate to correct the full GLAO field. A minimum of three is required to provide compensation over the field in both dimensions, but the question arises as to whether even more will yield substantial improvements. Consequently, we investigated the level of tilt correction with two guide star geometries: both used five Sodium LGS on a circle of 10 arcmin diameter, with either 3 or 8 NGS arranged as a regular polygon on the same circle. We found that 3 NGS are adequate as the magnitude of the FWHM improvement by using 8 NGS was only 10% greater than when 3 NGS were used (i.e. for a $\sim 0.1''$ decrease in the GLAO FWHM, increasing the number of NGS substantially decreased the FWHM by just $\sim 0.01''$).

7. SUMMARY

We have used the best available measures of ground layer turbulence profiles and a suite of modeling tools to study the performance of a GLAO system. This work is the most complete study of GLAO to date, and our results serve to “de-mystify” GLAO. Among the many results of this study, we highlight the following:

- The shape of the GLAO PSF is qualitatively the same as a seeing-limited PSF. Therefore, while having complete knowledge of the PSF is desirable, the FWHM of the PSF is a practical and useful general metric for measuring GLAO performance. Other performance metrics are more appropriate for specific applications, i.e.,

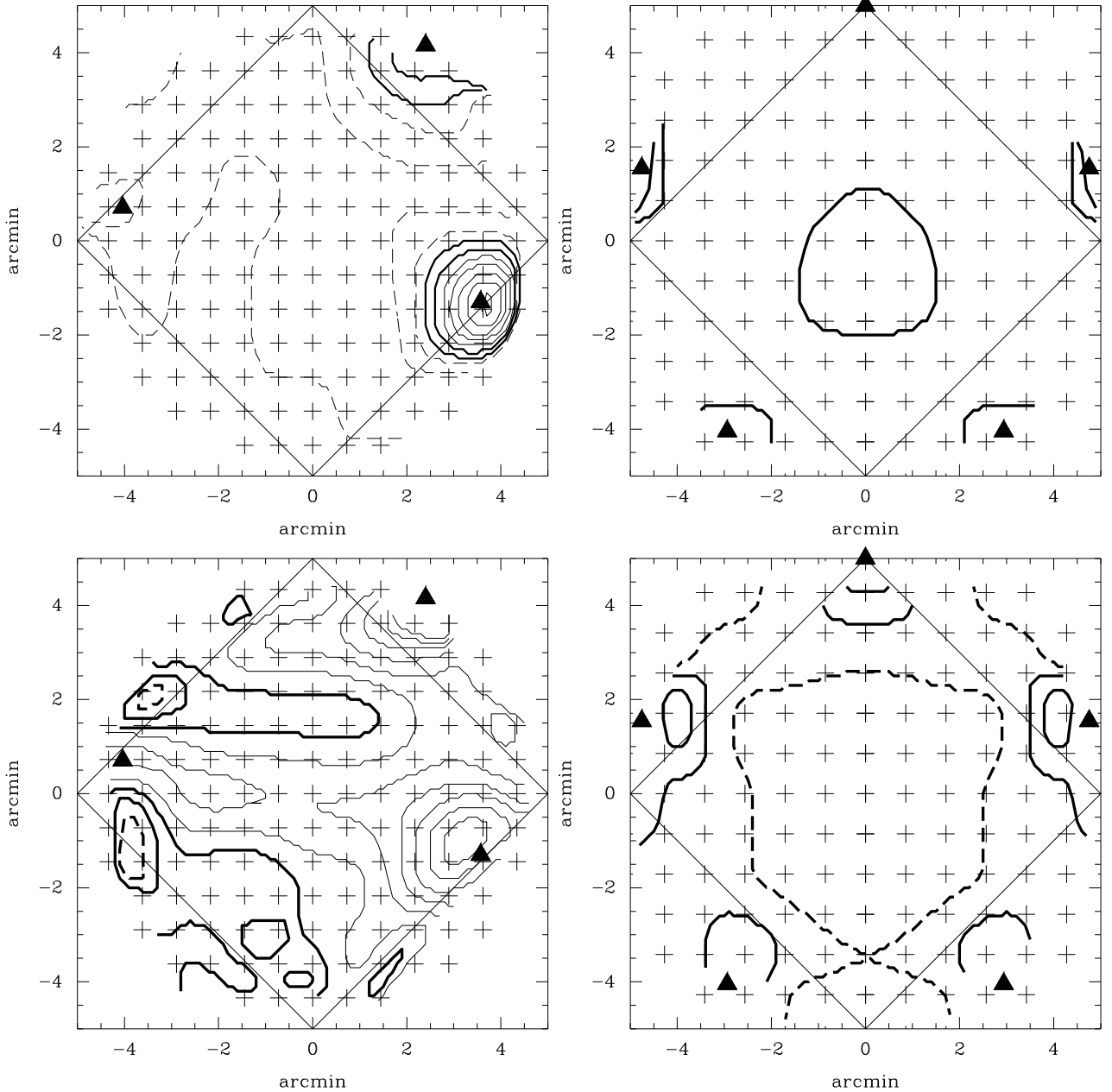


FIG. 19.— Comparison of GLAO correction using three NGSs of different brightnesses scattered randomly over the field (Left Panels) or five LGSs arranged in a regular pentagon (Right Panels). For each guide star asterism (marked with filled triangles), we show contours of FWHM (top panels) and ellipticity (bottom panels). The FWHM is smaller when LGS are used (both top panels have the same contours marked with heavy lines); the contours, separated by $0.02''$, show the NGS correction is between $0.02''$ and $0.04''$ worse over the majority of the FOV. More importantly for PSF calibration, the shape of the PSF is uniform when a regular asterism is used. In the ellipticity figures, the lowest measured ellipticity contour ($1 - b/a = 0.02$ of the PSF measured at the FWHM) is marked with a dashed solid line and is a good description for most of the FOV when LGS are used. The ellipticity in the PSF is as high as 0.14 within the FOV for the NGS case (contours are separated by 0.02 in ellipticity). Locations of the simulated PSFs are marked by plus signs, and a 7×7 square arcminutes FOV is marked on each figure as well.

Integration Time Ratio is ideal for background-limited imaging and ensquared energy is the most useful metric for spectroscopic observations.

- A GLAO system would significantly improve the image quality statistics. Unlike traditional AO systems, some of the greatest gains to be had with GLAO are obtained when the seeing is poor. In effect, this means that the number of nights with image quality worse than the current 70% level should be drastically reduced.

- Because diffraction limited imaging is not the goal of

GLAO, almost complete sky coverage is obtainable and the corresponding laser power requirements for a GLAO system are low.

- The performance of a GLAO system is relatively insensitive to a large number of trades. The performance is not a strong function of the corrected FOV, the actuator density of the DM, the conjugate height of the DM, height of the LGS, or the guide star geometry.

- While our GLAO modeling of very wide fields showed that performance gains are not as large as previously

reported, the substantial gains we do find would translate into major increases in the number of scientific programs that can be completed in a given time on large telescopes. Installing a GLAO system on a large telescope would increase the observing efficiency by at most 40%.

• GLAO is highly complementary to other modes of AO. GLAO can improve image quality in the optical and under intrinsically poor image quality conditions where more traditional AO systems are unusable, especially if a system with several hundred degrees of freedom is implemented. GLAO also yields the greatest survey efficiency; as we have shown, the survey efficiency of a GLAO system continues to increase with the FOV and should be

much greater than the MCAO survey efficiency. MCAO and classical AO could be used with a GLAO survey instrument for follow-up observations of the most exciting targets. In addition, the sky coverage of a GLAO system will be greater than that of traditional AO systems due to the increased FOV and the insensitivity of the performance to most of the studied variables.

The authors wish to thank S. Shectman for his useful comments and Gemini Observatory and its staff for their contributions.

REFERENCES

Babcock, H.W. 1953, PASP, 65, 229
 Bahcall, J.N., Soneira, R.M., 1980, *ApJ Supplement*, 44, 73
 Baranec, C.J., Lloyd-Hart, M., Codona, J.L., Milton, N.M. 2003, SPIE, 5169, 341
 Beckers, J.M. 1989, The NOAO 8-M Telescope Technical Description, Vol 2.
 Beckers, J. 2000, SPIE, 4007, 1056
 Dekany, R., Bouchez, A., Britton, M., Velur, V., Mitchell, T., Shelton, J.C., Roberts, J. 2006, SPIE, 6272, 627209
 Flicker, R., Rigaut, F.J., & Ellerbroek, B.L. 2000, SPIE, 4007, 1032
 Foy, R. & Labeyrie, A. 1985, A&A, 152, L29
 Fusco, T., Conan, J.-M., Michau, V., Mugnier, L.M., Rousset, G. 1999, Optics Letters, 24, 1472
 Hubin, N.N., *et al.* 2004, SPIE, 5490, 846
 Johnston, D.C. & Welsh, B.M. 1991, SPIE, 1542, 76
 Jolissaint, L., & Véran, J.-P. 2002, in ESO Conf. Proc. 58, "Beyond conventional adaptive optics," ed. E. Vernet *et al.*, (Garching: ESO), 201
 Jolissaint, L., Véran, J.-P., & Conan, R. 2006, accepted in J. Opt. Soc. Am. A
 Jolissaint, L., Véran, J.P., & Stoesz, J.A. 2004, SPIE, 5382, 468
 Le Louarn, M. 2002, MNRAS, 334, 865
 Le Louarn, M. & Hubin, N. 2004, MNRAS, 349, 1009
 Lloyd-Hart, M. & Milton, N. M. 2003, SPIE, 4840, 18
 Moffat, A.F.J. 1969, A&A, 3, 455
 Nicolle, M., Fusco, T., Michau, V., Rousset, G., Beuzit, J.-L. 2006, JOSA A, 23, 2333
 Ragazzoni, R. 1999, in ESO Conf. Proc. 56, "Astronomy with Adaptive Optics," ed. D. Bonaccini, (Garching: ESO), 651
 Ragazzoni, R., Farinato, J., & Marchetti, E. 2000, SPIE, 4007, 1076
 Rigaut, F., Véran, J.-P. & Lai, O. 1998, SPIE, 3353, 1038
 Rigaut, F. 2002, in ESO Conf. Proc. 58, "Beyond Conventional Adaptive Optics," ed. E. Vernet *et al.* (Garching: ESO), 11
 Stoesz, J.A., Jolissaint, L., Véran, J.-P., LeDue, J. 2004, SPIE, 5490, 713
 Tokovinin, A. 2003, MNRAS, 340, 52
 Tokovinin, A., Baumont, S., Vasquez, J. 2003, MNRAS, 340, 52
 Tokovinin, A. 2004, PASP, 116, 941
 Tokovinin, A. & Travouillon, T. 2006, MNRAS, 365, 1235
 Vernin, J. *et al.* 2000, Gemini RPT-AO-G0094